Available online at www.sciencedirect.com
SCIENCE DIRECT®
Journal of Sound and Vibration 286 (2005) 799–816
JOURNAL OF SOUND AND VIBRATION
www.elsevier.com/locate/jsvi

Three-dimensional free vibrations of a circular arch using the theory of a Cosserat point

M.B. Rubin[a,*], E. Tufekci[b]

[a]*Faculty of Mechanical Engineering, Technion - Israel Institute of Technology, Technion City, 32000 Haifa, Israel*
[b]*Faculty of Mechanical Engineering, Istanbul Technical University, Gumussuyu TR-80191, Istanbul, Turkey*

Received 19 December 2003; received in revised form 14 October 2004; accepted 19 October 2004
Available online 7 January 2005

Abstract

Small deformation three-dimensional free vibrations of a circular arch with uniform rectangular cross-section have been investigated by using different theoretical approaches and by experimental verification. Special emphasis has been focused on a numerical formulation which models each element of the arch using the theory of a Cosserat point. Comparison has been made with accurate three-dimensional numerical modeling of the arch using the computer program ANSYS. Also, three-dimensional beam elements in the computer programs ANSYS and I-DEAS have been considered along with an exact solution of approximate model equations of the arch. The results indicate that appropriate modeling of rotary inertia is necessary to predict accurate frequencies associated with torsional out-of-plane modes. Moreover, in its general form the theory of a Cosserat point is a fully nonlinear theory that has already been tested for buckling of beams and arches. Therefore, the success of the Cosserat theory for the dynamic problem considered in this paper suggests that the theory of a Cosserat point can be used for more complicated nonlinear dynamic problems of thin rod-like structures.

1. Introduction

A number of models of thin rods (curved beams) have been developed over the years. For example, equations for static large deformations and small deformation vibrations of rods can be

*Corresponding author. Tel.: +972 4 829 3188; fax: +972 4 829 5711.
E-mail addresses: mbrubin@tx.technion.ac.il (M.B. Rubin), tufekcie@itu.edu.tr (E. Tufekci).

0022-460X/$ - see front matter © 2004 Elsevier Ltd. All rights reserved.
doi:10.1016/j.jsv.2004.10.019

found in Ref. [1]. Also, Kuo and Yang [2] have reviewed a number of approaches for buckling of curved rods and presented an approach for deriving equations for a curved beam taking the limit of an infinite number of infinitesimal straight beam elements. A more modern approach to the mechanics of thin structures is based on Cosserat theories. These Cosserat theories are inherently nonlinear and are valid for both static and dynamic response of rods. Specifically, the theory of rods proposed by Antman [3,4] includes axial extension and tangential shear deformation of the rod's cross-section. More general equations which also include normal cross-sectional extension and cross-sectional shear deformation have been developed by Green et al. [5,6]. Also, the recent book by Rubin [7] discusses the Cosserat theories of shells, rods and points in a unified manner.

Modern applications of rod theory to micro-electro-mechanical-systems (MEMS) devices often require the ability to model both geometric nonlinearity and dynamics. Since the dynamic nonlinear response of a rod is characterized by partial differential equations which are functions of one space variable and time t, numerical methods must be developed to obtain solutions to general practical problems. Simo [8] and Simo and Vu-Quoc [9,10] have developed numerical methods for the rod theory proposed by Antman [3]. More recently Rubin [11] has developed a theory of a Cosserat point which is used to formulate the numerical solution of dynamic nonlinear problems of rods of the type proposed by Green et al. [5,6]. The theory of a Cosserat point is a fully nonlinear continuum theory which models the response of a small region like a finite element. Within the context of this theory the rod is replaced by a finite set of connected elements, each of which is modeled using the theory of a Cosserat point. As in the standard finite element formulation, neighboring Cosserat points are connected by kinematic and kinetic conditions at their common boundaries. Also, since the theory of a Cosserat point is fully nonlinear it can be used to model the dynamic stiffening that occurs in rotating turbine and helicopter blades.

The theory of a Cosserat point for rods has been tested by considering the static post-buckling behavior of nonlinear elastic beams and three-dimensional frames [12]. It has also been tested for static nonlinear problems of rods [13] and for the static post-buckling response of shallow arches [14]. The objective of this paper is to demonstrate that this theory of a Cosserat point can accurately model the dynamic response of rods. To this end, attention is focused on the simplest problem of small deformation free vibrations of a circular arch with a uniform rectangular cross-section.

The survey articles of Markus and Nanasi [15] and Chidamparam and Leissa [16] indicate that although in-plane vibrations of circular arches have been considered by a number of authors, studies of out-of-plane vibrations are much more rare. Some recent studies of out-of-plane vibrations include Refs. [17–21], where more references can be found.

After taking the displacements of a circular arch to be sinusoidal functions of time with frequency ω, the equations for the magnitudes of these displacements can be determined by the work by Tufekci and Arpaci [22] for in-plane deformations and by Tufekci and Dogruer [21] for out-of-plane deformations. Specifically, for in-plane deformations the equations of motion become

$$-\mu\omega^2 w = \frac{1}{R}\frac{\mathrm{d}R_t}{\mathrm{d}\phi} - \frac{R_n}{R}, \quad -\mu\omega^2 u = \frac{1}{R}\frac{\mathrm{d}R_n}{\mathrm{d}\phi} - \frac{R_t}{R}, \tag{1.1a,b}$$

$$-\mu\left[\frac{I_b}{A}\right]\omega^2\Omega_b = \frac{1}{R}\frac{\mathrm{d}M_b}{\mathrm{d}\phi} + R_n, \tag{1.1c}$$

with the constitutive equations

$$R_t = EA\left[\frac{1}{R}\frac{\mathrm{d}w}{\mathrm{d}\phi}+\frac{u}{R}\right], \quad R_n = \frac{GA}{k_n}\left[\frac{1}{R}\frac{\mathrm{d}u}{\mathrm{d}\phi}+\frac{w}{R}-\Omega_b\right], \tag{1.2a,b}$$

$$M_b = EI_b\left[\frac{1}{R}\frac{\mathrm{d}\Omega_b}{\mathrm{d}\phi}\right]. \tag{1.2c}$$

Also, for out-of-plane deformations the equations of motion are given by

$$-\mu\omega^2 v = \frac{1}{R}\frac{\mathrm{d}F_b}{\mathrm{d}\phi}, \quad -\mu\left[\frac{I_n}{A}\right]\omega^2\Omega_n = -F_b+\frac{M_t}{R}+\frac{1}{R}\frac{\mathrm{d}M_n}{\mathrm{d}\phi}, \tag{1.3a,b}$$

$$-\mu\left[\frac{I_p}{A}\right]\omega^2\Omega_t = -\frac{M_n}{R}+\frac{1}{R}\frac{\mathrm{d}M_t}{\mathrm{d}\phi}, \tag{1.3c}$$

with the constitutive equations

$$F_b = \frac{GA}{k_b}\left[\frac{1}{R}\frac{\mathrm{d}v}{\mathrm{d}\phi}+\Omega_n\right], \quad M_n = \frac{EI_n}{R}\left[\frac{\mathrm{d}\Omega_n}{\mathrm{d}\phi}+\Omega_t\right], \tag{1.4a,b}$$

$$M_t = \frac{GJ_p}{R}\left[\frac{\mathrm{d}\Omega_t}{\mathrm{d}\phi}-\Omega_n\right]. \tag{1.4c}$$

The notation used in these equations is the same as that in the references except that ρ in Ref. [22] has been changed to R and I_p in the expression for torsional stiffness in Ref. [21] has been corrected to J_p. For the calculations in Refs. [21,22] the values of the shear correction coefficients $\{k_n, k_b\}$ and the second moments of area $\{I_t, I_b, I_p\}$ and the quantity J_p related to the torsional stiffness were specified by (except that I_p was mistakenly set equal to J_p in Ref. [21])

$$k_n = k_b = \frac{6}{5}, \quad I_b = \frac{H^3W}{12}, \quad I_n = \frac{HW^3}{12}, \quad I_p = I_b + I_n, \tag{1.5a,b,c,d}$$

$$J_p = \frac{H^2W^2}{3}B(\xi_3), \quad B(\xi_3) = \frac{1}{\xi_3}\left[1-\frac{0.63}{\xi_3}\left\{1-\frac{1}{12\xi_3^4}\right\}\right], \quad \xi_3 = \mathrm{Max}\left\{\frac{H}{W},\frac{W}{H}\right\}, \tag{1.5e,f,g}$$

where H is the radial thickness and W is the axial depth of the rod's cross-section (Fig. 1). Moreover, it can be seen that the in-plane and out-of-plane equations are uncoupled and that torsion and bending are coupled in the out-of-plane modes. This is due to the fact that these equations are based on thin rod theory and they ignore warping of the cross-section.

In the following analysis it will be shown that it is essential to distinguish between the rotary inertia term I_p in Eq. (1.3c) and the torsional stiffness term J_p in Eq. (1.4c) to obtain accurate out-of-plane frequencies and mode shapes. The fact that these two terms are equal for circular cross-sections has possibly lead to an incorrect specification of $I_p = J_p$ for noncircular cross-sections in some of the literature [18–21].

An outline of this paper is as follows. Section 2 presents a brief summary of the basic equations of the theory of a Cosserat point for rods. Section 3 describes the numerical procedure for connecting the N Cosserat points which are used to model the arch under consideration.

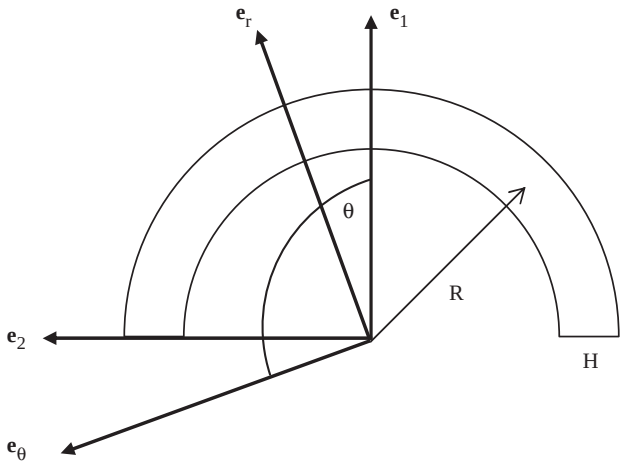

Fig. 1. Sketch of a circular arch with mean radius R and a rectangular cross-section of thickness H and width W.

Finally, Section 4 presents the experimental frequencies for free vibration of an arch with three different boundary conditions. Additional analytical [21,22] and numerical results are presented and discussed. Specifically, the Cosserat results are compared with converged calculations using three-dimensional brick elements in the commercial computer code ANSYS. Also, beam elements in ANSYS and another commercial computer code I-DEAS are considered.

Throughout the text, bold faced symbols are used to denote vector and tensor quantities. Also, $\mathbf{I}$ denotes the unity tensor; $\mathrm{tr}(\mathbf{A})$ denotes the trace of the second-order tensor $\mathbf{A}$ and $\mathbf{A}^{\mathrm{T}}$ denotes the transpose of $\mathbf{A}$. The scalar $\mathbf{a}\cdot\mathbf{b}$ denotes the dot product between two vectors $\mathbf{a}, \mathbf{b}$; the scalar $\mathbf{A}\cdot\mathbf{B} = \mathrm{tr}(\mathbf{A}\mathbf{B}^{\mathrm{T}})$ denotes the dot product between two second-order tensors $\mathbf{A}$, $\mathbf{B}$; the vector $\mathbf{a} \times \mathbf{b}$ denotes the cross product between $\mathbf{a}$ and $\mathbf{b}$; and the second-order tensor $\mathbf{a} \otimes \mathbf{b}$ denotes the tensor product between $\mathbf{a}$ and $\mathbf{b}$. Moreover, the usual summation convention over repeated lower-cased indices is implied with the range of Greek indices always being (1,2). The range of Latin indices will usually be (1,2,3) but sometimes it will be $(0, 1, \ldots, 5)$. Consequently, the range will be explicitly stated whenever it is not clear from the context. Moreover, there is no sum implied when the indices are upper-cased letters.

2. Basic equations of the theory of a Cosserat point

For the numerical solution of dynamic problems of rods, the rod is divided into N elements. Here, the Ith element ($I = 1, \ldots, N$) is modeled using the theory of a Cosserat point [11] and the equations of motion of the entire rod are obtained by using kinematic and kinetic coupling conditions at the common boundaries of the elements. These coupling equations yield a set of ordinary differential equations which are functions of time t only. This section briefly summarizes the basic ideas with additional details being recorded in Refs. [7,11–13,23].

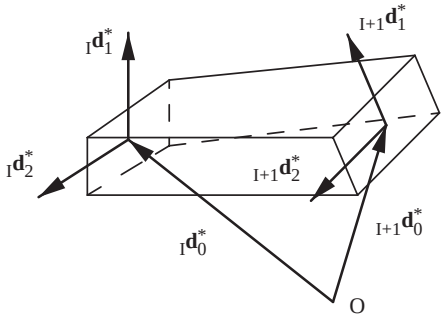

Fig. 2. Sketch of the deformed configuration of the Ith Cosserat point.

Fig. 2 shows a sketch of the deformed configuration of the Ith Cosserat point. Specifically, the Ith cross-section $(I = 1, 2, \ldots, N+1)$ is characterized by three nodal director vectors $\{{}_I\mathbf{d}_0^*, {}_I\mathbf{d}_1^*, {}_I\mathbf{d}_2^*\}$, with ${}_I\mathbf{d}_0^*$ locating its centroid (relative to a fixed origin O), and $\{{}_I\mathbf{d}_1^*$ and ${}_I\mathbf{d}_2^*\}$ identifying deformable line elements in the cross-section. In addition to the usual three rotational degrees of freedom of the cross-section, the nodal directors $\{{}_I\mathbf{d}_1^*$ and ${}_I\mathbf{d}_2^*\}$ include: cross-sectional extension (i.e. the lengths of ${}_I\mathbf{d}_1^*$ and ${}_I\mathbf{d}_2^*$ are allowed to change) and cross-sectional shear deformation (i.e. the angle between ${}_I\mathbf{d}_1^*$ and ${}_I\mathbf{d}_2^*$ is allowed to change). Kinematic coupling requires the nodal directors of the $(I-1)$th element to be the same as those of the Ith element at their common boundary. In the stress-free reference configuration these nodal directors take the reference values $\{{}_I\mathbf{D}_0^*, {}_I\mathbf{D}_1^*, {}_I\mathbf{D}_2^*\}$.

Here, attention is confined to rods which have uniform rectangular cross-sections, with thickness H and width W. The reference directors ${}_I\mathbf{D}_i$ are related to the reference nodal directors ${}_I\mathbf{D}_i^*$ by the expressions

$$
\begin{aligned}
{}_I\mathbf{D}_0 &= \frac{1}{2}({}_I\mathbf{D}_0^* + {}_{I+1}\mathbf{D}_0^*), \quad {}_I\mathbf{D}_3 = \frac{1}{{}_IL}({}_{I+1}\mathbf{D}_0^* - {}_I\mathbf{D}_0^*),\\
{}_I\mathbf{D}_1 &= \frac{1}{2}({}_I\mathbf{D}_1^* + {}_{I+1}\mathbf{D}_1^*), \quad {}_I\mathbf{D}_4 = \frac{1}{{}_IL}({}_{I+1}\mathbf{D}_1^* - {}_I\mathbf{D}_1^*),\\
{}_I\mathbf{D}_2 &= \frac{1}{2}({}_I\mathbf{D}_2^* + {}_{I+1}\mathbf{D}_2^*), \quad {}_I\mathbf{D}_5 = \frac{1}{{}_IL}({}_{I+1}\mathbf{D}_2^* - {}_I\mathbf{D}_2^*),
\end{aligned}
\tag{2.1}
$$

where the length ${}_IL$ of the Ith element is determined by

$$
|{}_I\mathbf{D}_3| = 1, \quad {}_IL = |{}_{I+1}\mathbf{D}_0^* - {}_I\mathbf{D}_0^*|. \tag{2.2}
$$

For the linearized theory the present values ${}_I\mathbf{d}_i^*$ of the nodal directors and present values ${}_I\mathbf{d}_i$ of the element directors are expressed in terms of the nodal displacements ${}_I\boldsymbol{\delta}_i^*$ and the director displacements ${}_I\boldsymbol{\delta}_i$, such that

$$
{}_I\mathbf{d}_i^* = {}_I\mathbf{D}_i^* + {}_I\boldsymbol{\delta}_i^* \text{ for } i = 0, 1, 2, \quad {}_I\mathbf{d}_i = {}_I\mathbf{D}_i + {}_I\boldsymbol{\delta}_i \text{ for } i = 0, 1, \ldots, 5. \tag{2.3}
$$

Also, ${}_I\boldsymbol{\delta}_i$ are related to ${}_I\boldsymbol{\delta}_i^*$ through equations of type (2.1)

$$
\begin{aligned}
{}_I\boldsymbol{\delta}_0 &= \frac{1}{2}({}_I\boldsymbol{\delta}_0^* + {}_{I+1}\boldsymbol{\delta}_0^*), \quad {}_I\boldsymbol{\delta}_3 = \frac{1}{{}_IL}({}_{I+1}\boldsymbol{\delta}_0^* - {}_I\boldsymbol{\delta}_0^*),\\
{}_I\boldsymbol{\delta}_1 &= \frac{1}{2}({}_I\boldsymbol{\delta}_1^* + {}_{I+1}\boldsymbol{\delta}_1^*), \quad {}_I\boldsymbol{\delta}_4 = \frac{1}{{}_IL}({}_{I+1}\boldsymbol{\delta}_1^* - {}_I\boldsymbol{\delta}_1^*),\\
{}_I\boldsymbol{\delta}_2 &= \frac{1}{2}({}_I\boldsymbol{\delta}_2^* + {}_{I+1}\boldsymbol{\delta}_2^*), \quad {}_I\boldsymbol{\delta}_5 = \frac{1}{{}_IL}({}_{I+1}\boldsymbol{\delta}_2^* - {}_I\boldsymbol{\delta}_2^*).
\end{aligned}
\tag{2.4}
$$

Moreover, these displacements are determined by solving the balances of director momentum

$$
\sum_{j=0}^{5} {}_Im\,{}_Iy^{ij}\,{}_I\ddot{\boldsymbol{\delta}}_j = {}_Im\,{}_I\mathbf{b}^i - {}_I\mathbf{t}^i \quad \text{for } i = 0,1,\ldots,5,
\tag{2.5}
$$

with

$$
{}_I\mathbf{t}^0 = 0, \quad {}_Im\,{}_I\mathbf{b}^i = {}_Im\,{}_I\mathbf{B}^i + {}_I\mathbf{m}_1^i + {}_I\mathbf{m}_2^i \quad \text{for } i = 0,1,\ldots,5.
\tag{2.6}
$$

In these equations, ${}_Im$ is the mass of the element, ${}_Iy^{ij}$ are director inertia coefficients, ${}_I\mathbf{B}^i$ are the specific (per unit mass) external assigned director couples due to body force and tractions on the lateral surface of the element, $\{{}_I\mathbf{m}_1^0, {}_I\mathbf{m}_2^0\}$ are resultant forces and $\{{}_I\mathbf{m}_1^\alpha, {}_I\mathbf{m}_2^\alpha, \alpha = 1,2\}$ are directors couples which are applied to the ends of the element, and ${}_I\mathbf{t}^i$ are intrinsic director couples which need to be specified by constitutive equations.

Furthermore, for the linear theory the displacements $\{{}_I\boldsymbol{\delta}_i^*, {}_I\boldsymbol{\delta}_i\}$ and the kinetic quantities

$$
\{{}_I\mathbf{t}^i, {}_I\mathbf{B}^i, {}_I\mathbf{m}_1^i, {}_I\mathbf{m}_2^i\}
\tag{2.7}
$$

are assumed to be small enough that quadratic terms in these quantities can be neglected. Also, it is convenient to introduce the reciprocal vectors ${}_I\mathbf{D}^i$

$$
{}_I\mathbf{D}_i \cdot {}_I\mathbf{D}^j = \delta_1^j \quad \text{for } i,j = 1,2,3,
\tag{2.8}
$$

where δ_1^j is the Kronecker delta symbol. Then, the homogeneous strain tensor ${}_I\mathbf{E}$ and the inhomogeneous strains ${}_I\boldsymbol{\beta}_\alpha$ can be defined by

$$
{}_I\mathbf{E} = \sum_{i=1}^{3} \frac{1}{2}[{}_I\boldsymbol{\delta}_i \otimes {}_I\mathbf{D}^i + {}_I\mathbf{D}^i \otimes {}_I\boldsymbol{\delta}_i],
$$

$$
{}_I\boldsymbol{\beta}_1 = {}_I\boldsymbol{\delta}_4 - ({}_I\mathbf{D}^i \cdot {}_I\mathbf{D}_4)\,{}_I\boldsymbol{\delta}_i, \quad {}_I\boldsymbol{\beta}_2 = {}_I\boldsymbol{\delta}_5 - ({}_I\mathbf{D}^i \cdot {}_I\mathbf{D}_5)\,{}_I\boldsymbol{\delta}_i.
\tag{2.9}
$$

Next, with reference to the fixed rectangular Cartesian base vectors $\mathbf{e}_i$ $(i = 1,2,3)$ and the cylindrical polar base vectors $\{\mathbf{e}_r, \mathbf{e}_\theta, \mathbf{e}_3\}$

$$
\mathbf{e}_r(\theta) = \cos\,\theta\;\mathbf{e}_1 + \sin\,\theta\;\mathbf{e}_2, \quad \mathbf{e}_\theta(\theta) = -\sin\,\theta\;\mathbf{e}_1 + \cos\,\theta\;\mathbf{e}_2,
\tag{2.10}
$$

consider a circular arch of mean radius R, which occupies the region $-\beta \leqslant \theta \leqslant \beta$, and is divided into N equal sections so that the reference nodal directors ${}_I\mathbf{D}_i^*$ are given by

$$ {}_I\mathbf{D}_0^* = R\mathbf{e}_r(\theta_I^*), \quad {}_I\mathbf{D}_1^* = \mathbf{e}_r(\theta_I^*), \quad {}_I\mathbf{D}_2^* = -\mathbf{e}_3,$$

$$\theta_I^* = -\beta + 2(I-1)\alpha, \quad \bar{\theta}_I^* = \frac{1}{2}[\theta_I^* + \theta_{I+1}^*], \quad \alpha = \frac{\beta}{N} \quad \text{for } I = 1, 2, \ldots, N+1, \tag{2.11}$$

where $\theta = \theta_I^*$ is the angle locating the Ith cross-section and $\theta = \bar{\theta}_I^*$ is the angle locating the center of the Ith element. It then follows from Eq. (2.1) that

$$ {}_I\mathbf{D}_0 = R\cos\alpha\mathbf{e}_r(\bar{\theta}_I^*), \quad {}_I\mathbf{D}_1 = \cos\alpha\mathbf{e}_r(\bar{\theta}_I^*), \quad {}_I\mathbf{D}_2 = -\mathbf{e}_3, \quad {}_I\mathbf{D}_3 = \mathbf{e}_\theta(\bar{\theta}_I^*),$$

$$ {}_I\mathbf{D}_4 = \frac{1}{R}\mathbf{e}_\theta(\bar{\theta}_I^*), \quad {}_I\mathbf{D}_5 = 0, \tag{2.12}$$

where the length ${}_IL$ defined in Eq. (2.2) is given by

$$ {}_IL = L = 2R\sin\alpha. \tag{2.13}$$

Moreover, it follows from Eqs. (2.1) and (2.8) that

$$ {}_ID^{1/2} = \cos\alpha, \quad {}_I\mathbf{D}^1 = \frac{1}{\cos\alpha}\mathbf{e}_r(\bar{\theta}_I^*), \quad {}_I\mathbf{D}^2 = -\mathbf{e}_3, \quad {}_I\mathbf{D}^3 = \mathbf{e}_\theta(\bar{\theta}_I^*). \tag{2.14}$$

Now, for an arch made of a uniform, homogeneous isotropic elastic material, the mass ${}_Im$ and the scalar ${}_IV$ can be expressed in terms of the constant three-dimensional reference density ρ_0^* and the geometry, such that

$$ {}_Im = m = \rho_0^* HWL\cos\alpha = \rho_0^* HWR\sin(2\alpha), \quad {}_IV = V = HWL. \tag{2.15}$$

Moreover, the strain energy function ${}_I\Sigma$ for the Cosserat point can be expressed in terms of the strain energy function Σ^* of the three-dimensional material and the strain energy function ${}_I\Psi$ associated with inhomogeneous deformations, such that

$$ {}_I\Sigma = {}_I\Sigma({}_I\mathbf{E}, {}_I\boldsymbol{\beta}_\alpha) = \Sigma^*({}_I\mathbf{E}) + {}_I\Psi({}_I\boldsymbol{\beta}_\alpha),$$

$$\rho_0^*\Sigma^*({}_I\mathbf{E}) = \frac{1}{2}K^*({}_I\mathbf{E}\cdot\mathbf{I})^2 + \mu^*({}_I\mathbf{E}'\cdot{}_I\mathbf{E}'), \quad {}_I\mathbf{E}' = {}_I\mathbf{E} - \frac{1}{3}({}_I\mathbf{E}\cdot\mathbf{I})\mathbf{I}, \tag{2.16}$$

where K^* is the bulk modulus, μ^* is the shear modulus, ${}_I\mathbf{E}'$ is the deviatoric strain, ${}_I\Psi$ is given by [7,11,23]

$$\begin{aligned} {}_Im\,{}_I\Psi = \frac{1}{2}{}_ID^{1/2}V[&K_1({}_I\kappa_1^3)^2 + K_2({}_I\kappa_2^3)^2 + K_3({}_I\kappa_1^1)^2 + 2K_4({}_I\kappa_1^1{}_I\kappa_2^2) + K_5({}_I\kappa_2^2)^2 \\ &+ K_6({}_I\kappa_1^2)^2 + 2K_7({}_I\kappa_1^2{}_I\kappa_2^1) + K_8({}_I\kappa_2^1)^2], \end{aligned}$$

$$ {}_I\kappa_1^1 = {}_IL_I\boldsymbol{\beta}_1\cdot{}_I\mathbf{D}^1, \quad {}_I\kappa_1^2 = W_I\boldsymbol{\beta}_1\cdot{}_I\mathbf{D}^2, \quad {}_I\kappa_1^3 = H_I\boldsymbol{\beta}_1\cdot{}_I\mathbf{D}^3,$$

$$ {}_I\kappa_2^1 = H_I\boldsymbol{\beta}_2\cdot{}_I\mathbf{D}^1, \quad {}_I\kappa_2^2 = L_I\boldsymbol{\beta}_2\cdot{}_I\mathbf{D}^2, \quad {}_I\kappa_2^3 = W_I\boldsymbol{\beta}_2\cdot{}_I\mathbf{D}^3 \tag{2.17}$$

and $\{K_1–K_8\}$ are constants that characterize the stiffness of the element. These constants have been determined by matching exact solutions of a parallelepiped for pure bending and torsion [23] to obtain

$$K_1 = K_2 = \frac{E^*}{12}, \quad K_3 = K_5 = \frac{E^*}{12(1-\nu^{*2})}, \quad K_4 = \frac{\nu^* E^*}{12(1-\nu^{*2})},$$

$$K_6 = \frac{H}{W}\left[\frac{\mu^* b^*(\xi_3)}{6(2-K)}\right], \quad K_7 = \left[\frac{\mu^* b^*(\xi_3)(K-1)}{6(2-K)}\right], \quad K_8 = \frac{W}{H}\left[\frac{\mu^* b^*(\xi_3)}{6(2-K)}\right],$$

$$K = \text{Min}\left[2-\varepsilon, \frac{1}{b^*(\xi_3)}\sqrt{\frac{{}_I L^2 b^*(\xi_1) b^*(\xi_2)}{HW}}\right], \quad \varepsilon = 0.1,$$

$$\xi_1 = \text{Max}\left\{\frac{W}{{}_I L}, \frac{{}_I L}{W}\right\}, \quad \xi_2 = \text{Max}\left\{\frac{H}{{}_I L}, \frac{{}_I L}{H}\right\}, \quad \xi_3 = \text{Max}\left\{\frac{H}{W}, \frac{W}{H}\right\},$$

$$b^*(\xi) = \frac{1}{\xi}\left[1 - \frac{192}{\pi^5 \xi}\sum_{n=1}^{\infty}\left[\frac{1}{(2n-1)^5}\right]\tanh\left\{\frac{\pi(2n-1)\xi}{2}\right\}\right], \tag{2.18}$$

in terms of Young's modulus E^*, and Poisson's ratio ν^*, which are related to K^* and μ^* by

$$K^* = \frac{2\mu^*(1+\nu^*)}{3(1-2\nu^*)}, \quad E^* = 2\mu^*(1+\nu^*). \tag{2.19}$$

Also, $b^*(\xi)$ is a function characterizing the torsional stiffness and ε is a small constant that is used to ensure that the strain energy due to torsion remains positive definite. In this regard, it is noted that the approximate function $B(\xi)$ in Eq. (1.5f) is remarkably close to the exact form $b^*(\xi)$ in Eq. (2.18) for the full range of ξ.

For an elastic Cosserat point, the constitutive equations become

$${}_I D^{1/2}\,{}_I\mathbf{T} = {}_I m \frac{\partial_I \Sigma}{\partial_I \mathbf{E}}, \quad {}_I\mathbf{t}^4 = {}_I m \frac{\partial_I \Sigma}{\partial_I \boldsymbol{\beta}_1}, \quad {}_I\mathbf{t}^5 = {}_I m \frac{\partial_I \Sigma}{\partial_I \boldsymbol{\beta}_2}. \tag{2.20}$$

Thus, with the help of Eqs. (2.16) and (2.17) it follows that

$${}_I\mathbf{T} = V[K^*({}_I\mathbf{E}\cdot\mathbf{I})\mathbf{I} + 2\mu^*\,{}_I\mathbf{E}'],$$

$${}_I\mathbf{t}^4 = {}_I D^{1/2} V[{}_I L\{K_3\,{}_I\kappa_1^1 + K_4\,{}_I\kappa_2^2\}\,{}_I\mathbf{D}^1 + W\{K_6\,{}_I\kappa_1^2 + K_7\,{}_I\kappa_2^1\}\,{}_I\mathbf{D}^2 + H\{K_1\,{}_I\kappa_1^3\}\,{}_I\mathbf{D}^3],$$

$${}_I\mathbf{t}^5 = {}_I D^{1/2} V[H\{K_7\,{}_I\kappa_1^2 + K_8\,{}_I\kappa_2^1\}\,{}_I\mathbf{D}^1 + {}_I L\{K_4\,{}_I\kappa_1^1 + K_5\,{}_I\kappa_2^2\}\,{}_I\mathbf{D}^2 + W\{K_2\,{}_I\kappa_2^3\}\,{}_I\mathbf{D}^3],$$

$${}_I\mathbf{t}^i = [{}_I D^{1/2}\,{}_I\mathbf{T} - {}_I\mathbf{t}^4 \otimes {}_I\mathbf{D}_4 - {}_I\mathbf{t}^5 \otimes {}_I\mathbf{D}_5]\cdot {}_I\mathbf{D}^i \quad \text{for } i = 1,2,3. \tag{2.21}$$

More specifically, using Eqs. (2.9), (2.12) and (2.14), it can be shown that for a circular arch

$$
{}_I\mathbf{E} = \frac{1}{2}\left[\frac{1}{\cos\alpha}\{{}_I\boldsymbol{\delta}_1 \otimes \mathbf{e}_r(\bar{\theta}_I^*) + \mathbf{e}_r(\bar{\theta}_I^*) \otimes {}_I\boldsymbol{\delta}_1\} - \{{}_I\boldsymbol{\delta}_2 \otimes \mathbf{e}_3 + \mathbf{e}_3 \otimes {}_I\boldsymbol{\delta}_2\}\right.
$$
$$
\left. + \{{}_I\boldsymbol{\delta}_3 \otimes \mathbf{e}_\theta(\bar{\theta}_I^*) + \mathbf{e}_\theta(\bar{\theta}_I^*) \otimes {}_I\boldsymbol{\delta}_3\}\right], \quad {}_I\boldsymbol{\beta}_1 = {}_I\boldsymbol{\delta}_4 - \frac{1}{R}\,{}_I\boldsymbol{\delta}_3, \quad {}_I\boldsymbol{\beta}_2 = {}_I\boldsymbol{\delta}_5,
$$

$$
{}_I\mathbf{t}^1 = V[K^*({}_I\mathbf{E}\cdot\mathbf{I})\mathbf{I} + 2\mu^*\,{}_I\mathbf{E}']\mathbf{e}_r(\bar{\theta}_I^*), \quad {}_I\mathbf{t}^2 = -V\cos\alpha[K^*({}_I\mathbf{E}\cdot\mathbf{I})\mathbf{I} + 2\mu^*\,{}_I\mathbf{E}']\mathbf{e}_3,
$$

$$
{}_I\mathbf{t}^3 = V\cos\alpha[K^*({}_I\mathbf{E}\cdot\mathbf{I})\mathbf{I} + 2\mu^*\,{}_I\mathbf{E}']\mathbf{e}_\theta(\bar{\theta}_I^*) - \frac{1}{R}\,{}_I\mathbf{t}^4,
$$

$$
{}_I\mathbf{t}^4 = V\cos\alpha\left[{}_IL\{K_3\,{}_I\kappa_1^1 + K_4\,{}_I\kappa_2^2\}\frac{1}{\cos\alpha}\,\mathbf{e}_r(\bar{\theta}_I^*) - W\{K_6\,{}_I\kappa_1^2 + K_7\,{}_I\kappa_2^1\}\mathbf{e}_3 + H\{K_1\,{}_I\kappa_1^3\}\mathbf{e}_\theta(\bar{\theta}_I^*)\right],
$$

$$
{}_I\mathbf{t}^5 = V\cos\alpha\left[H\{K_7\,{}_I\kappa_1^2 + K_8\,{}_I\kappa_2^1\}\frac{1}{\cos\alpha}\,\mathbf{e}_r(\bar{\theta}_I^*) - {}_IL\{K_4\,{}_I\kappa_1^1 + K_5\,{}_I\kappa_2^2\}\mathbf{e}_3 + W\{K_2\,{}_I\kappa_2^3\}\mathbf{e}_\theta(\bar{\theta}_I^*)\right]. \tag{2.22}
$$

Next, the director inertia coefficients are specified by

$$
{}_Iy^{00} = 1, \quad {}_Iy^{11} = (1-\alpha_y)\left[\frac{H^2}{\pi^2}\right] + \alpha_y\left[\frac{H^2}{12}\right], \quad {}_Iy^{22} = (1-\alpha_y)\left[\frac{W^2}{\pi^2}\right] + \alpha_y\left[\frac{W^2}{12}\right],
$$

$$
{}_Iy^{33} = \frac{{}_IL^2}{\pi^2}, \quad {}_Iy^{01} = {}_Iy^{10} = \gamma_1\frac{H^2}{\pi^2 R}, \quad {}_Iy^{34} = {}_Iy^{43} = \frac{\gamma_2}{R}\left[\frac{2L}{3\pi}\right]^4,
$$

$$
{}_Iy^{44} = {}_Iy^{55} = \gamma_3\left[\frac{2L}{3\pi}\right]^4 \quad \text{all other } {}_Iy^{ij} = 0 \text{ for } i,j = 0,1,\ldots,5. \tag{2.23}
$$

In these expressions for ${}_Iy^{11}$ and ${}_Iy^{22}$, α_y is a parameter that is used to help match free vibrational frequencies. Specifically, for $\alpha_y = 0$ these values correspond to those which have been determined by matching predictions of free vibrations of a parallelepiped [24], and for $\alpha_y = 1.0$ these values are consistent with those for a rigid cross-section. To determine limitations on the value of α_y, the

expression for the kinetic energy ${}_I\mathscr{K}$ of the Ith element is expanded to obtain

$$
\begin{aligned}
{}_I\mathscr{K} &= \sum_{i=0}^{5}\sum_{j=0}^{5}\frac{1}{2}\,m_I y^{ij}\,{}_I\mathbf{w}_j\cdot{}_I\mathbf{w}_j \\
&= \frac{1}{2}\,m\left[\left\{{}_I\mathbf{w}_0+\frac{H^2}{\pi^2R}\,{}_I\mathbf{w}_1\right\}\cdot\left\{{}_I\mathbf{w}_0+\frac{H^2}{\pi^2R}\,{}_I\mathbf{w}_1\right\}\right. \\
&\quad+\frac{H^2}{\pi^2}\left\{(1-\alpha_y)+\alpha_y\,\frac{\pi^2}{12}-\frac{H^2}{\pi^2R^2}\right\}{}_I\mathbf{w}_1\cdot{}_I\mathbf{w}_1+\frac{W^2}{\pi^2}\left\{(1-\alpha_y)+\alpha_y\,\frac{\pi^2}{12}\right\}{}_I\mathbf{w}_2\cdot{}_I\mathbf{w}_2 \\
&\quad+\frac{L^2}{\pi^2}\left\{{}_I\mathbf{w}_3+\frac{16L^2}{81\pi^2R}\,{}_I\mathbf{w}_4\right\}\cdot\left\{{}_I\mathbf{w}_3+\frac{16L^2}{81\pi^2R}\,{}_I\mathbf{w}_4\right\} \\
&\quad\left.+\left[\frac{2L}{3\pi}\right]^4\left\{1-\frac{16L^2}{81\pi^2R^2}\right\}{}_I\mathbf{w}_4\cdot{}_I\mathbf{w}_4+\left[\frac{2L}{3\pi}\right]^4{}_I\mathbf{w}_5\cdot{}_I\mathbf{w}_5\right].
\end{aligned}
\tag{2.24}
$$

Thus, since m is positive the restrictions

$$
0\leqslant\alpha_y\leqslant 1,\quad \frac{16L^2}{81\pi^2R}<1 \tag{2.25}
$$

are sufficient conditions for the kinetic energy to remain a positive definite function of the director velocities. Moreover, in Eq. (2.25) use has been made of Eq. (2.13) and the fact that $H\leqslant R/2$.

3. Numerical solution procedure

For the numerical solution procedure it is convenient to use Eq. (2.13), the director inertia coefficients (2.23), and the results (B.8) in Ref. [11]

$$
{}_I\mathbf{m}_1^3=-\frac{L}{2}\,{}_I\mathbf{m}_1^0,\quad {}_I\mathbf{m}_2^3=\frac{L}{2}\,{}_I\mathbf{m}_2^0,\quad {}_I\mathbf{m}_1^4=-\frac{L}{2}\,{}_I\mathbf{m}_1^1,\quad {}_I\mathbf{m}_2^4=\frac{L}{2}\,{}_I\mathbf{m}_2^1,
$$

$$
{}_I\mathbf{m}_1^5=-\frac{L}{2}\,{}_I\mathbf{m}_1^2,\quad {}_I\mathbf{m}_2^5=\frac{L}{2}\,{}_I\mathbf{m}_2^2, \tag{3.1}
$$

to reformulate the equations of motion (2.5) in the alternative forms

$$
{}_I\mathbf{m}_1^0=\frac{1}{L}\left[\frac{L}{2}\{{}_I m({}_I\ddot{\boldsymbol{\delta}}_0+{}_I y^{01}\,{}_I\ddot{\boldsymbol{\delta}}_1)-{}_I m_I\mathbf{B}^0\}-\{{}_I m({}_I y^{33}\,{}_I\ddot{\boldsymbol{\delta}}_3+{}_I y^{34}\,{}_I\ddot{\boldsymbol{\delta}}_4)-{}_I m_I\mathbf{B}^3+{}_I\mathbf{t}^3\}\right],
$$

$$
{}_I\mathbf{m}_2^0=\frac{1}{L}\left[\frac{L}{2}\{{}_I m({}_I\ddot{\boldsymbol{\delta}}_0+{}_I y^{01}\,{}_I\ddot{\boldsymbol{\delta}}_1)-{}_I m_I\mathbf{B}^0\}+\{{}_I m({}_I y^{33}\,{}_I\ddot{\boldsymbol{\delta}}_3+{}_I y^{34}\,{}_I\ddot{\boldsymbol{\delta}}_4)-{}_I m_I\mathbf{B}^3+{}_I\mathbf{t}^3\}\right],
$$

$$
{}_I\mathbf{m}_1^1=\frac{1}{L}\left[\frac{L}{2}\{{}_I m({}_I y^{10}\,{}_I\ddot{\boldsymbol{\delta}}_0+{}_I y^{11}\,{}_I\ddot{\boldsymbol{\delta}}_1)-{}_I m_I\mathbf{B}^1+{}_I\mathbf{t}^1\}-\{{}_I m({}_I y^{43}\,{}_I\ddot{\boldsymbol{\delta}}_3+{}_I y^{44}\,{}_I\ddot{\boldsymbol{\delta}}_4)-{}_I m_I\mathbf{B}^4+{}_I\mathbf{t}^4\}\right],
$$

$$
{}_I\mathbf{m}_2^1 = \frac{1}{L}\left[\frac{L}{2}\{{}_I m({}_I y^{10}\,{}_I\ddot{\boldsymbol{\delta}}_0 + {}_I y^{11}\,{}_I\ddot{\boldsymbol{\delta}}_1) - {}_I m_I\mathbf{B}^1 + {}_I\mathbf{t}^1\} + \{{}_I m({}_I y^{43}\,{}_I\ddot{\boldsymbol{\delta}}_3 + {}_I y^{44}\,{}_I\ddot{\boldsymbol{\delta}}_4) - {}_I m_I\mathbf{B}^4 + {}_I\mathbf{t}^4\}\right],
$$

$$
{}_I\mathbf{m}_1^2 = \frac{1}{L}\left[\frac{L}{2}\{{}_I m_I y^{22}\,{}_I\ddot{\boldsymbol{\delta}}_2 - {}_I m_I\mathbf{B}^2 + {}_I\mathbf{t}^2\} - \{{}_I m_I y^{55}\,{}_I\ddot{\boldsymbol{\delta}}_5 - {}_I m_I\mathbf{B}^5 + {}_I\mathbf{t}^5\}\right],
$$

$$
{}_I\mathbf{m}_2^2 = \frac{1}{L}\left[\frac{L}{2}\{{}_I m_I y^{22}\,{}_I\ddot{\boldsymbol{\delta}}_2 - {}_I m_I\mathbf{B}^2 + {}_I\mathbf{t}^2\} + \{{}_I m_I y^{55}\,{}_I\ddot{\boldsymbol{\delta}}_5 - {}_I m_I\mathbf{B}^5 + {}_I\mathbf{t}^5\}\right]. \tag{3.2}
$$

Next, the equations of motion of the entire arch are obtained by using kinematic and kinetic coupling equations at the interior nodes ($I = 2, 3, \ldots, N$). Specifically, the kinematic coupling equations are satisfied by expressions (2.4). Furthermore, the kinetic coupling equations associated with the interior nodes require [7]

$$
{}_{I-1}\mathbf{m}_2^i + {}_I\mathbf{m}_1^i = {}_I\mathbf{M}^{i*} \quad \text{for } I = 2, 3, \ldots, N \text{ and } i = 0, 1, 2, \tag{3.3}
$$

where $({}_I\mathbf{M}^{0*})$ are concentrated forces and $({}_I\mathbf{M}^{\alpha*})$ are director couples applied to the nodes. Details of the physical meanings of these concentrated loads can be found in Ref. [12]. Also, the boundary conditions require specification of

$$
\{{}_1\boldsymbol{\delta}_0^* \text{ or } {}_1\mathbf{m}_1^0\} \text{ and } \{{}_1\boldsymbol{\delta}_1^* \text{ or } {}_1\mathbf{m}_1^1\} \text{ and } \{{}_1\boldsymbol{\delta}_2^* \text{ or } {}_1\mathbf{m}_1^2\},
$$

$$
\{{}_{N+1}\boldsymbol{\delta}_0^* \text{ or } {}_N\mathbf{m}_2^0\} \text{ and } \{{}_{N+1}\boldsymbol{\delta}_1^* \text{ or } {}_N\mathbf{m}_2^1\} \text{ and } \{{}_{N+1}\boldsymbol{\delta}_2^* \text{ or } {}_N\mathbf{m}_2^2\}. \tag{3.4}
$$

Eqs. (3.3) and (3.4) represent $3(N + 1)$ ordinary differential vector equations to determine the $3(N + 1)$ nodal vector displacements ${}_I\boldsymbol{\delta}_i^*$ as functions of time. Since these equations are second order in time it is necessary to specify the initial values of

$$
\{{}_I\boldsymbol{\delta}_i^*(0), {}_I\dot{\boldsymbol{\delta}}^*{}_i(0)\} \quad \text{for } i = 0, 1, 2. \tag{3.5}
$$

More specifically, for particular values of the nodal director displacements ${}_I\boldsymbol{\delta}_i^*$, the director displacements ${}_I\boldsymbol{\delta}_i$ are determined by Eq. (2.4), the intrinsic director couples ${}_I\mathbf{t}^i$ are determined by the constitutive equations (2.21), and the contact director couples $\{{}_I\mathbf{m}_1^i, {}_I\mathbf{m}_2^i\}$ are determined by Eq. (3.2). In this regard, it is emphasized that although $\{{}_I\mathbf{m}_1^0, {}_I\mathbf{m}_2^0\}$ represent forces applied to the ends of the Ith element, the couples $\{{}_I\mathbf{m}_1^\alpha, {}_I\mathbf{m}_2^\alpha\}$ are more general than the standard mechanical moments ${}_I\mathbf{m}_\alpha$ applied about the centroid of the cross-sections of the Ith element, which are defined by

$$
{}_I\mathbf{m}_1 = {}_I\mathbf{D}_1^* \times {}_I\mathbf{m}_1^1 + {}_I\mathbf{D}_2^* \times {}_I\mathbf{m}_1^2,
$$

$$
{}_I\mathbf{m}_2 = {}_{I+1}\mathbf{D}_1^* \times {}_I\mathbf{m}_2^1 + {}_{I+1}\mathbf{D}_2^* \times {}_I\mathbf{m}_2^2 \quad \text{for } I = 1, 2, \ldots, N. \tag{3.6}
$$

To be more specific, clamped conditions at the end $I = N + 1$ are specified by

$$
{}_{N+1}\boldsymbol{\delta}_i^*(t) = 0 \quad \text{for } i = 0, 1, 2 \tag{3.7}
$$

and free conditions are specified by

$$
{}_N\mathbf{m}_2^i(t) = 0 \quad \text{for } i = 0, 1, 2. \tag{3.8}
$$

4. Experiments, analysis and discussion

Experiments were performed to measure the free vibrational frequencies of a semi-circular arch with three types of boundary conditions. The arch was made of steel with the measured material properties given by

$$E^* = 90.0\,\text{GPa}, \quad \nu^* = 0.30, \quad \rho_0^* = 7.85\,\text{Mg/m}^3. \tag{4.1}$$

Also, the dimensions of the arch were determined by averaging 12 measurements taken at equally spaced circumferential intervals to obtain (see Fig. 1)

$$R = 0.20\,\text{m}, \quad H = 0.034\,\text{m}, \quad W = 0.021\,\text{m}. \tag{4.2}$$

The output of an accelerometer attached to the arch was used to identify peak frequencies associated with free vibrational modes, but the associated mode shapes were not measured. The results are recorded for three sets of boundary conditions in Table 1 (free–free), Table 2 (clamped–free) and Table 3 (clamped–clamped).

Numerical calculations were performed using ANSYS and converged solutions based on the three-dimensional 20-node brick element Solid95 and the 8-node brick element Solid45 are given in Tables 1–3. The meshes for these calculations used 128 elements circumferentially, eight elements through the radial thickness (H), and four elements through the axial width (W). For comparison purposes the total number of degrees of freedom (dof) are indicated for each calculation. Also, the ANSYS calculation using the element Solid95 was considered to be the most accurate result and all other calculations were normalized relative to the ANSYS Solid95 values by introducing the error e in the frequency ω defined by

$$e = \frac{\omega}{\omega(\text{Solid95})} - 1. \tag{4.3}$$

It can be seen from Tables 1–3 that the calculations are reasonably consistent with the experimental results for all three boundary conditions. Also, the results of the ANSYS Solid45 element are consistent with those of the Solid95 element. These tables include results of numerical calculations of three beam models and the Cosserat theory (for two values of α_y), which were each meshed with 128 elements circumferentially. In addition, they include the exact solution of Eqs. (1.1)–(1.4) denoted by T&A [22] and T&D [21]. The last column in these tables uses the specifications (1.5), and the second to last column uses the specifications (1.5) with the rotary inertia specified by

$$I_p = J_p, \tag{4.4}$$

instead of by Eq. (1.5e). This exact solution and the other beam models include the effects of: (a) axial extension; (b) tangential shear deformation; and (c) rotary inertia, but not the effects of: (d) normal cross-sectional extension; and (e) cross-sectional shear deformation, which are also included in the Cosserat model. Specifically, the ANSYS Beam4 model allows for specification of the stiffnesses and rotary inertia terms independently like in Eqs. (1.1)–(1.4). For the Beam-Linear and the Beam-Parabolic elements in I-DEAS these stiffnesses and inertia terms are calculated automatically by the program. Moreover, the Beam-Parabolic element in I-DEAS is an isoparametric element which attempts to model curved structures and which can be attached to parabolic shell elements.

Table 1
Frequencies for free–free boundary conditions

Mode No.	Mode type (Plane)	Exp. (Hz)	ANSYS Solid95 $8*4*120$ dof 64,107 (Hz)	ANSYS Solid45 $8*4*120$ dof 17,415 e (%)	ANSYS Beam4 128 dof 774 e (%)	I-DEAS Beam-Linear 128 dof 774 e (%)	I-DEAS Beam-Parabolic 128 dof 1542 e (%)	Cosserat $\alpha_y = 0.0$ $N = 128$ dof 1161 e (%)	Cosserat $\alpha_y = 0.95$ $N = 128$ dof 1161 e (%)	T&A T&D $I_p = J_p$ e (%)	T&A T&D e (%)
1	In	252	241	0.03	−0.29	−0.29	−0.22	−0.27	−0.19	−0.30	−0.30
2	Out	340	346	0.55	0.26	0.25	1.01	−0.51	−0.11	0.71	0.25
3	In	688	686	0.07	−0.64	−0.65	−0.46	−0.19	0.01	−0.65	−0.65
4	Out	744	712	0.31	0.44	0.44	4.43	−2.14	−0.05	3.28	0.43
5	Out	1352	1309	0.54	0.28	0.27	4.19	−5.41	0.01	3.59	0.26
6	Out	1376	1332	0.12	0.02	0.01	[a]	−4.42	−0.42	[a]	0.00
7	In	1496	1400	0.13	−0.77	−0.78	−0.46	−0.10	0.25	−0.79	−0.79
	Out[b]	—	—	—	—	—	—	—	—	1544[b]	—
8	Out	2140	1934	0.60	−0.40	−0.40	−20.36	−6.49	−0.44	15.18	−0.41
9	Out	2340	2214	0.44	0.42	0.41	0.27	−1.23	0.31	2.84	0.40
	Out[c]	—	—	—	—	—	2292[c]	—	—	—	—
10	In	2480	2320	0.21	−0.88	−0.88	−0.41	0.04	0.55	−0.89	−0.89

Commercial code results, Cosserat results, in-plane solutions [22] (T&A) and out-of-plane solutions [21] (T&D).

[a]I-DEAS Beam-Parabolic element misses the out-of-plane mode number 6.

[b]The frequency (Hz) associated with an incorrect out-of-plane mode predicted by (T&D) with an incorrect specification of rotary inertia.

[c]The frequency associated with an incorrect out-of-plane mode predicted by I-DEAS Beam-Parabolic element. The error parameter e is defined in Eq. (4.3).

Table 2
Frequencies for clamped–free boundary conditions

Mode No.	Mode type (Plane)	Exp. (Hz)	ANSYS Solid95 $8*4*120$ dof 63,744 (Hz)	ANSYS Solid45 $8*4*120$ dof 17,280 e (%)	ANSYS Beam4 128 dof 768 e (%)	I-DEAS Beam-Linear 128 dof 768 e (%)	I-DEAS Beam-Parabolic 128 dof 1536 e (%)	Cosserat $\alpha_y = 0.0$ $N = 128$ dof 1152 e (%)	Cosserat $\alpha_y = 0.95$ $N = 128$ dof 1152 e (%)	T&A T&D $I_p = J_p$ e (%)	T&A T&D e (%)
1	Out	35.2	35.1	0.80	−0.71	−0.72	−0.72	−0.68	0.12	−0.71	−0.72
2	In	57.6	57.5	0.05	−0.10	−0.10	−0.09	−0.52	−0.08	−0.11	−0.11
3	Out	108	111	0.35	−0.05	−0.06	−0.01	−0.75	−0.19	0.07	−0.07
4	In	184	180	0.08	−0.62	−0.63	−0.61	−0.46	−0.16	−0.64	−0.64
5	Out	372	373	0.38	0.02	0.02	0.76	−0.82	−0.13	0.49	0.01
6	In	601	599	0.12	−0.73	−0.74	−0.62	−0.20	−0.06	−0.74	−0.74
7	Out	801	811	0.36	0.26	0.26	1.82	−1.08	−0.01	1.38	0.25
8	In	1250	1293	0.17	−0.97	−0.98	−0.78	0.08	0.02	−0.99	−0.99
9	Out	1304	1308	0.42	−0.08	−0.09	5.82	−0.08	0.01	5.53	−0.09
10	Out	1544	1613	0.32	0.03	0.03	11.46	−3.84	−0.01	11.83	0.02

Commercial code results, Cosserat results, in-plane solutions [22] (T&A) and out-of-plane solutions [21] (T&D). The error parameter e is defined in Eq. (4.3).

Table 3
Frequencies for clamped–clamped boundary conditions

Mode No.	Mode type (Plane)	Exp. (Hz)	ANSYS Solid95 $8*4*120$ dof 63,381 (Hz)	ANSYS Solid45 $8*4*120$ dof 17,145 e (%)	ANSYS Beam4 128 dof 762 e (%)	I-DEAS Beam-Linear 128 dof 762 e (%)	I-DEAS Beam-Parabolic 128 dof 1530 e (%)	Cosserat $\alpha_y = 0.0$ $N = 128$ dof 1143 e (%)	Cosserat $\alpha_y = 0.95$ $N = 128$ dof 1143 e (%)	T&A T&D $I_p = J_p$ e (%)	T&A T&D e (%)
1	Out	145	149	0.17	−0.49	−0.49	−0.50	−0.78	−0.73	−0.44	−0.50
2	Out	448	425	0.25	−0.08	−0.09	0.14	−0.57	−0.44	0.05	−0.09
3	In	568	555	0.15	−0.97	−0.97	−0.94	−0.17	−0.13	−0.98	−0.98
4	Out	876	877	0.31	0.04	0.03	0.09	−0.40	−0.20	0.20	0.02
5	In	1176	1143	0.18	−1.15	−1.15	−1.06	0.22	0.33	−1.16	−1.16
6	Out	1504	1477	0.41	0.09	0.08	0.03	−0.23	0.05	0.27	0.08
7	Out	1864	1998	0.63	−1.21	−1.22	[a]	−9.93	−1.23	10.79	−1.22
8	In	1960	2068	0.26	−1.16	−1.16	−0.98	0.45	0.67	−1.17	−1.17
9	Out	2033	2208	0.52	0.10	0.09	−0.20	−0.06	0.32	8.37	0.08
10	In	2256	2416	0.09	−0.65	−0.66	−0.56	0.10	0.19	−0.66	−0.66

Commercial code results, Cosserat solutions, in-plane solutions [22] (T&A) and out-of-plane solutions [21] (T&D).

[a]I-DEAS Beam-Parabolic element misses the out-of-plane mode number 7. The error parameter e is defined in Eq. (4.3).

The calculations of the Cosserat theory were performed using the program Matlab. For free vibrations, body force is neglected, the lateral surfaces of the arch are free from surface tractions, and the concentrated loads ${}_I\mathbf{M}^{i*}$ vanish so that

$$ {}_I\mathbf{B}^i = 0, \quad {}_I\mathbf{M}^{i*} = 0. \tag{4.5}$$

Next, by specifying the nodal director displacements in the forms

$$ {}_I\boldsymbol{\delta}_i^*(t) = {}_I\bar{\boldsymbol{\delta}}_i^* \sin(\omega t) \tag{4.6}$$

the equations of motion (3.3) and the boundary conditions (3.7), (3.8) yield a system of linear algebraic equations for the unknown amplitudes ${}_I\bar{\boldsymbol{\delta}}_i^*$, with the coefficient matrix being a function of the vibrational frequency ω. Then, standard analysis yields the natural frequencies and shapes of the vibrational modes predicted by the discrete model. In particular, it is noted that these natural frequencies depend on the specification of the parameter α_y in Eq. (2.23) for the director inertia coefficients.

In all tables the deformation is considered to be in-plane or out-of-plane if the $({}_I\mathbf{D}_2 \otimes {}_I\mathbf{D}_3)$ component of the strain tensor ${}_I\mathbf{E}$ (i.e. the out-out plane component of the rod's center line) in the Cosserat solution is zero or nonzero, respectively. Furthermore, it is noted that the out-of-plane modes include a significant amount of torsional deformation.

From these tables it can be seen that the largest errors in the Cosserat solution with $\alpha_y = 0$ occur for the out-of-plane modes 5, 6, 8 in the free–free case, and the out-of-plane mode 7 for the clamped–clamped case. An attempt was made to reduce this error by adjusting the value of α_y in Eq. (2.23) until the error for the out-of-plane mode 5 in the free–free case nearly vanished. With this value of $\alpha_y = 0.95$ it can be seen that the Cosserat solutions for $N = 128$ predict accurate results for the first 10 frequencies for all three boundary conditions since the error is limited to around 1.0%. Additional calculations were performed which indicate that the Cosserat solution is reasonably well converged for $N = 32$.

With regard to the specification of $\alpha_y = 0.95$, it should be recalled that within the context of the direct approach to the Cosserat theory the director inertia coefficients need to be specified by constitutive equations. The determination of the values of these coefficients in Ref. [24] by comparison with exact solutions for vibrations of a rectangular parallelepiped indicates that these coefficients actually characterize the distribution of inertia in specific modes and not just the distribution of mass in the rod's cross-section. Moreover, the stiffness to torsion of a beam with a rectangular cross-section was used to determine the constitutive coefficient for static torsion in the arch [11]. This coefficient accounts for the softening effect of warping of the cross-section even though the Cosserat theory does not model the kinematics of warping explicitly. For the torsional vibrations of the arch under consideration here it is expected that the effect of warping of the cross-section is reduced since there is limited time for stress relief to propagate from the boundaries. This suggests that the actual stiffness to torsional vibration should be higher than that to static torsion, especially for the higher modes. Although this cannot be modeled directly in the Cosserat theory without warping it is possible to model the effect on the free vibrational frequency by adjusting the constant α_y. Specifically, by setting $\alpha_y = 0.95$, the effective inertia of the cross-section to torsion is decreased, which compensates for the softer static stiffness, resulting in an

improved match with the free vibrational frequency of torsional modes. Furthermore, it is interesting to note that the frequencies of many of the modes of vibration are nearly unaffected by this modification of the director inertia coefficients.

As mentioned earlier, the Beam-Linear and the Beam-Parabolic elements in I-DEAS automatically calculate the values of the quantities

$$\{I_b, I_n, I_p, J_p\}. \tag{4.7}$$

When the cross-section of the beam is specified to be rectangular, I-DEAS calculates the correct values (1.5) of Eq. (4.7). In particular, the results in Tables 1–3 indicate that when the stiffnesses and rotary inertia terms are specified by Eq. (1.5), the exact solution (T&A and T&D), ANSYS Beam4 and I-DEAS Beam-Linear element predict accurate results for all three boundary conditions. However, the Beam-Parabolic element in I-DEAS predicts inaccurate results for out-of-plane modes even though it has more degrees of freedom than the Beam-Linear element. Furthermore, it is seen that the use of the incorrect specification of the rotary inertia (4.4) in the analytical solution causes significant errors in the predictions of out-of-plane modes 8 in Table 1 and 9 and 10 in Table 2, which are similar to the errors predicted by the element I-DEAS Beam-Parabolic. This suggests that the source of the error in the Beam-Parabolic element might be related to incorrect modeling of rotary inertia.

5. Conclusions

In conclusion, small deformation three-dimensional free vibrations of a circular arch with uniform rectangular cross-section have been investigated by using different theoretical approaches and by experimental verification. The results indicate that when the value of rotary inertia is properly specified, the theory of a Cosserat point, the exact solution of Tufekci and Arpaci [22] and Tufekci and Dogruer [21], the Beam4 element in ANSYS and the Beam-Linear element in I-DEAS are all capable of predicting accurate values of the frequencies of free vibration for all three boundary conditions considered. However, the Beam-Parabolic element in I-DEAS predicts inaccurate frequencies for out-of-plane modes.

Moreover, in its general form [11] the theory of a Cosserat point is a fully nonlinear theory that has already been tested for buckling of beams [12] and arches [14]. Therefore, the success of the Cosserat theory for the dynamic problem considered in this paper suggests that the theory of a Cosserat point can be used for more complicated nonlinear dynamic problems like those of rotating turbine and helicopter blades.

Acknowledgements

The authors would like to acknowledge O. Ozdemirci's help with the commercial code calculations.

References

[1] A.E.H. Love, *A Treatise on the Mathematical Theory of Elasticity*, Dover, New York, 1944.
[2] S.R. Kuo, Y.B. Yang, New theory on bukling of curved beams, *ASCE Journal of Engineering Mechanics* 117 (1991) 1698–1717.
[3] S.S. Antman, The theory of rods, in: C. Truesdell (Ed.), *Handbuch der Physik*, vol. VIa/2, Springer, Berlin, 1972, pp. 641–703.
[4] S.S. Antman, *Nonlinear Problems of Elasticity*, Applied Mathematical Sciences, vol. 107, Springer, Berlin, 1995.
[5] A.E. Green, P.M. Naghdi, M.L. Wenner, On the theory of rods I: derivations from the three-dimensional equations, *Proceedings of the Royal Society of London A* 337 (1974) 451–483.
[6] A.E. Green, P.M. Naghdi, M.L. Wenner, On the theory of rods II: developments by direct approach, *Proceedings of the Royal Society of London A* 337 (1974) 485–507.
[7] M.B. Rubin, *Cosserat Theories*: *Shells*, *Rods and Points*, Solid Mechanics and its Applications, vol. 79, Kluwer, The Netherlands, 2000.
[8] J.C. Simo, A finite strain beam formulation. The three-dimensional dynamic problem. Part I, *Computer Methods in Applied Mechanics and Engineering* 49 (1985) 55–70.
[9] J.C. Simo, L. Vu-Quoc, A three-dimensional finite-strain rod model. Part II: computational aspects, *Computer Methods in Applied Mechanics and Engineering* 58 (1986) 79–116.
[10] J.C. Simo, L. Vu-Quoc, On the dynamics in space of rods undergoing large motions—a geometrically exact approach, *Computer Methods in Applied Mechanics and Engineering* 66 (1988) 125–161.
[11] M.B. Rubin, Numerical solution procedures for nonlinear elastic rods using the theory of a Cosserat point, *International Journal of Solids and Structures* 38 (2001) 4395–4437.
[12] B. Nadler, M.B. Rubin, Post-buckling behavior of nonlinear elastic beams and three-dimensional frames using the theory of a Cosserat point, *Mathematics and Mechanics of Solids* 9 (2004) 369–398.
[13] M.B. Rubin, Numerical solution procedures for nonlinear elastic curved rods using the theory of a Cosserat point, *Mathematics and Mechanics of Solids*, 2005, to appear.
[14] M.B. Rubin, Buckling of elastic shallow arches using the theory of a Cosserat point, *ASCE Journal of Engineering Mechanics* 130 (2004) 216–224.
[15] S. Markus, T. Nanasi, Vibration of curved beams, *The Shock and Vibration Digest* 13 (1981) 3–14.
[16] P. Chidamparam, A.W. Leissa, Vibrations of planar curved beams, rings and arches, *Applied Mechanics Reviews* 46 (1993) 467–483.
[17] W.P. Howson, A.K. Jemah, Exact out-of-plane natural frequencies of curved Timoshenko beams, *ASCE Journal of Engineering Mechanics* 125 (1999) 19–25.
[18] S.Y. Lee, J.C. Chao, Out-of-plane vibrations of curved non-uniform beams of constant radius, *Journal of Sound and Vibration* 238 (2000) 443–458.
[19] S.Y. Lee, J.C. Chao, Exact solutions for out-of-plane vibration of curved nonuniform beams, *ASME Journal of Applied Mechanics* 68 (2001) 186–191.
[20] Y.-B. Yang, C.-M. Wu, J.-D. Yau, Dynamic response of horizontally curved beam subjected to vertical and horizontal moving loads, *Journal of Sound and Vibration* 242 (2001) 519–537.
[21] E. Tufekci, O.Y. Dogruer, Exact solution of out-of-plane free vibrations of a circular beam with uniform cross-section, *Proceedings of the Second International Conference on Structural Stability and Dynamics*, Singapore, 16–18 December, 2002, pp. 231–236.
[22] E. Tufekci, A. Arpaci, Exact solution of in-plane vibrations of circular arches with account taken of axial extension, transverse shear and rotary inertia effects, *Journal of Sound and Vibration* 209 (1998) 845–856.
[23] B. Nadler, M.B. Rubin, Determination of hourglass coefficients in the theory of a Cosserat point for nonlinear elastic beams, *International Journal of Solids and Structures* 40 (2003) 6163–6188.
[24] M.B. Rubin, Free vibration of a rectangular parallelepiped using the theory of a Cosserat point, *Journal of Applied Mechanics* 53 (1986) 45–50.